J Therm Spray Tech
https://doi.org/10.1007/s11666-019-00830-y

PEER REVIEWED

Preparation of MCrAlY–Al_2O_3 Composite Coatings with Enhanced Oxidation Resistance through a Novel Powder Manufacturing Process

Mingwen Bai[1] · Bo Song[1] · Liam Reddy[1] · Tanvir Hussain[1]

Submitted: 14 July 2018 / in revised form: 4 January 2019

Abstract MCrAlY–Al_2O_3 composite coatings were prepared by high-velocity oxygen fuel thermal spraying with bespoke composite powder feedstock for high-temperature applications. Powder processing via a suspension route was employed to achieve a fine dispersion of α-Al_2O_3 submicron particles on the MCrAlY powder surface. This was, however, compromised by ~ 50% less flowability of the feedstock during spraying. Nevertheless, the novel powder manufacturing process introduced in this study has shown potential as an alternative route to prepare tailored composite powder feedstock for the production of metal matrix composites. In addition, the newly developed MCrAlY–Al_2O_3 composite coatings exhibited superior oxidation resistance, compared to conventional MCrAlY coatings, with the formation of nearly exclusively Al_2O_3 scale after isothermal oxidation at 900 °C for 10 h. The addition of α-Al_2O_3 particles in the MCrAlY coatings as a second phase was found to have promoted the formation of YAG oxides ($Y_xAl_yO_z$) during spraying and also accelerated the outwards diffusion of Al, which resulted in enhanced oxidation resistance.

Keywords alumina · bond coat · HVOF · MCrAlY · oxidation · suspension

This article is an invited paper selected from presentations at the 2018 International Thermal Spray Conference, held May 7-10, 2018, in Orlando, Florida, USA, and has been expanded from the original presentation.

✉ Tanvir Hussain
tanvir.hussain@nottingham.ac.uk

[1] Faculty of Engineering, University of Nottingham, Nottingham NG7 2RD, UK

Introduction

Alumina-forming coatings, also known as bond coats, have been widely used on hot section of gas turbine engines since early 1960s (Ref 1-5). Among them, a bond coat system of MCrAlY (M = Ni/Co) alloy has been developed based on a balance among several aspects that include oxidation, corrosion and ductility (Ref 6-8). High-velocity oxygen fuel (HVOF) thermal spraying is one of the most widely used coating techniques for the deposition of MCrAlY coatings for high-temperature corrosion/oxidation protection (Ref 9-11). HVOF thermal-sprayed MCrAlY coatings are normally used within the temperature range of 950-1100 °C with the formation of a 1-10-μm-thick protective α-Al_2O_3 scale. This, however, creates a temperature gap for the use of MCrAlY bond coats in other high-temperature applications, e.g., ultra-supercritical (USC) steam boilers and turbines, and other turbomachinery for higher efficiencies and lower emissions, which are in operation at temperatures below 950 °C but in excess of 650 °C (Ref 12-14). No protective α-Al_2O_3 scale would form on the coating surfaces at these low temperatures as restricted by both kinetic and thermodynamic factors. Metastable θ- and γ-Al_2O_3 that are non-protective (voids) would form instead in the temperature range of 700-950 °C (Ref 15), which are also fast growing with oxidation rate constants (k_p) being 2-3 orders of magnitude higher than that of α-Al_2O_3.

Efforts have been made to develop MCrAlY-Al_2O_3 composite coatings with dispersion of Al_2O_3 particles on the surface as nucleation sites to promote the early formation of a coherent α-Al_2O_3 scale (Ref 16-20). The challenge is, however, there is no established process to prepare composite powder feedstock with a homogenous distribution of the second phase particles with submicron or nano-sizes that are prone to agglomeration (Ref 6). A

Published online: 23 January 2019

recent study by Bolelli et al. (Ref 21) produced NiCrAlY–Al_2O_3 composite coatings by a "hybrid" spraying technique with two injection nozzles feeding both dry NiCrAlY powder and a suspension of Al_2O_3 particles simultaneously into the gas stream. More recently, satelliting, as a manufacturing technique (Ref 22-25), was introduced to mix small quantities of hard reinforcing submicron or nanoparticles into larger volumes of soft metallic matrix powders. The "satellited" powders were obtained by mixing the two powders in a water solution containing 2.7 wt.% of polyvinyl alcohol (PVA) as a binder, followed by a drying process. This satelliting process has been patented (Ref 22), and it is now used for a wide range of composite manufacturing applications that involves powder feedstock, e.g., additive manufacturing and cold spraying (Ref 23-26). In this study, a similar powder mixing process via a suspension route was introduced with the aim to achieve a uniform distribution of Al_2O_3 submicron particles with MCrAlY powders, albeit without any binders. The composite feedstock powders were then sprayed onto stainless steels by conventional HVOF thermal spraying. The oxidation behavior of the composite coatings during isothermal heat treatment at 900 °C for 10 h was studied compared to the conventional MCrAlY coatings. The effect of the α-Al_2O_3 dispersion on the composite coatings' oxidation was also discussed.

Experiment

Powder and Substrate

A commercial MCrAlY powder for thermal spraying (Amdry9624, spheroidal, gas atomized, Oerlikon Metco, UK) was used as feedstock with a nominal composition of Ni Bal., Cr 21.0-23.0, Al 9.0-11.0, Y 0.8-1.2 wt.% and a nominal size distribution of $-37 + 11$ µm, mixed with a commercial alumina powder (CR1, 100% alpha, Baikowski, France) with a D50 particle size of 1 µm. The feedstock powders were sprayed onto AISI 304 stainless steels substrates (nominal composition Fe-19.0Cr-9.3 Ni-2.0Mn-0.05C wt.%) with a dimension of $60 \times 25 \times 2$ mm.

Preparation of Composite Feedstock

A suspension route was employed to prepare the composite feedstock without any additives. Ethanol denatured (industrial methylated spirit) with a concentration of ethanol over 99% in volume was used as the suspension medium. The mixing process was completed in less than 10 min on a hot plate at 150 °C with a magnetic stirring (500 rpm) until fully dried. An AS-300 Hall Flow Meter was used to test the flowability of the composite powder feedstock before spraying. The flowability of the composite powder feedstock was found to be poor, so equal weight of original MCrAlY powders was added to improve the flow rate of the composite feedstock and mixed in a rotary milling system (CAPCO Test Equipment 2VS, Suffolk, UK) at a speed of 250 rpm for less than 1 h—the conditions chosen did not change the particle size and shapes. The homogeneity of the final feedstock was checked under optical microscope. The final composite powder feedstock containing 5 wt.% of Al_2O_3 was then used for spraying.

HVOF Thermal Spray Process

Substrates were first grit blasted with brown alumina (F100, 0.125-0.149 mm) under 6 bar pressure and then cleaned by an ultrasonic acetone bath to remove any embedded alumina particles. The substrates were mounted onto a carousel rotating at 73 rpm with a vertical axis of rotation. Metjet IV, a liquid fuel-based HVOF thermal spray system (Metallisation Ltd., UK), was used for the deposition of the MCrAlY–Al_2O_3 composite and the conventional MCrAlY coatings with kerosene as the fuel. Both coatings were deposited with six passes under the same condition, and the samples were air-cooled during spraying. The length of the nozzle of the HVOF thermal spray gun was 100 mm, and a standoff distance of 356 mm was used during the spray runs. The flow rates of kerosene and oxygen were 476 mL/min and 900 L/min, respectively, giving a total flow rate of 28.2 g/s and 100% stoichiometry, while nitrogen was used a carrier gas for the powder. The as-sprayed samples were then cut into a dimension of $10 \times 10 \times 2$ mm and placed in alumina crucibles. Isothermal oxidation treatment was carried out at 900 °C for 10 h in a box furnace with a heating/cooling rate of 10 °C/min.

Characterization Methods

Scanning electron microscope with JEOL in-lens Schottky field emissions source (FEG-SEM, JEOL 7100F, USA) equipped with an energy-dispersive x-ray (EDX) detector (silicon drift detector size: 150 mm^2, Oxford Instruments, UK) was used to examine the feedstock powder, the coating surface and cross sections in secondary electron (SE) and back-scattered electron (BSE) modes. An x-ray diffractometer (XRD, D500 Siemens Germany) with Cu $K\alpha$ radiation (1.5406 Å) was used to identify the phases presented in the powders and coatings in the $20° \leq 2\theta \leq 90°$ range with a step size of 0.05° and dwell time of 2 s. For the oxidation analysis, the coating samples were mounted in epoxy resin filled with Ballotini glass beads for

low shrinkage, and the cross sections were cut and polished down to a 1 μm finish.

Thermo-Calc® Calculation

Thermodynamic calculation of oxidation products as a function of effective partial pressures of O_2 at 900 °C was carried out by Thermo-Calc® software (Version 2017b) with TCS Ni-based superalloys (TCNi8.1) database following CALPHAD (Computer Coupling of Phase Diagrams and Thermochemistry) (Ref 27, 28). The use of Thermo-Calc® on alumina-forming and chromia-forming alloys systems has been validated by our previous work (Ref 29, 30) and others (Ref 31-38).

Results

Composite Feedstock Powders

Figure 1 shows the representative morphologies of the composite feedstock powder with 10 wt.% of alumina as examined after drying. In comparison with the original MCrAlY feedstock (left), the composite feedstock exhibits a good dispersion of alumina submicron particles mainly attached on the surface of the MCrAlY surface with a radius ratio in the range of 40 ~ 80:1.

Figure 2 shows the combined and normalized XRD patterns of the composite feedstock powder with 10, 5 and 0 wt.% of alumina (from top to bottom). The MCrAlY powder is composed of a mixture of β-Ni(Al,Cr) phase and γ-Ni(Cr) phase with a minor impurity of Ni_2Al_3 and Ni_5Y phase. With the increase in the alumina content, the peak intensity of the α-alumina is observed to increase proportionally, while it became difficult to identify the α-alumina peaks when the α-alumina content was less than 5 wt.% (approximately equal to 2.7 mol.%), which might reach the detection limit of XRD analysis. This could be used as an effective indicator for the examination of the alumina content in the composite coatings using XRD analysis.

As-sprayed Composite Coatings

Figure 3 shows the XRD analysis of the as-sprayed composite coatings and the MCrAlY coatings. Both patterns are nearly identical comprising a majority of β and $\gamma(\gamma')$ phase

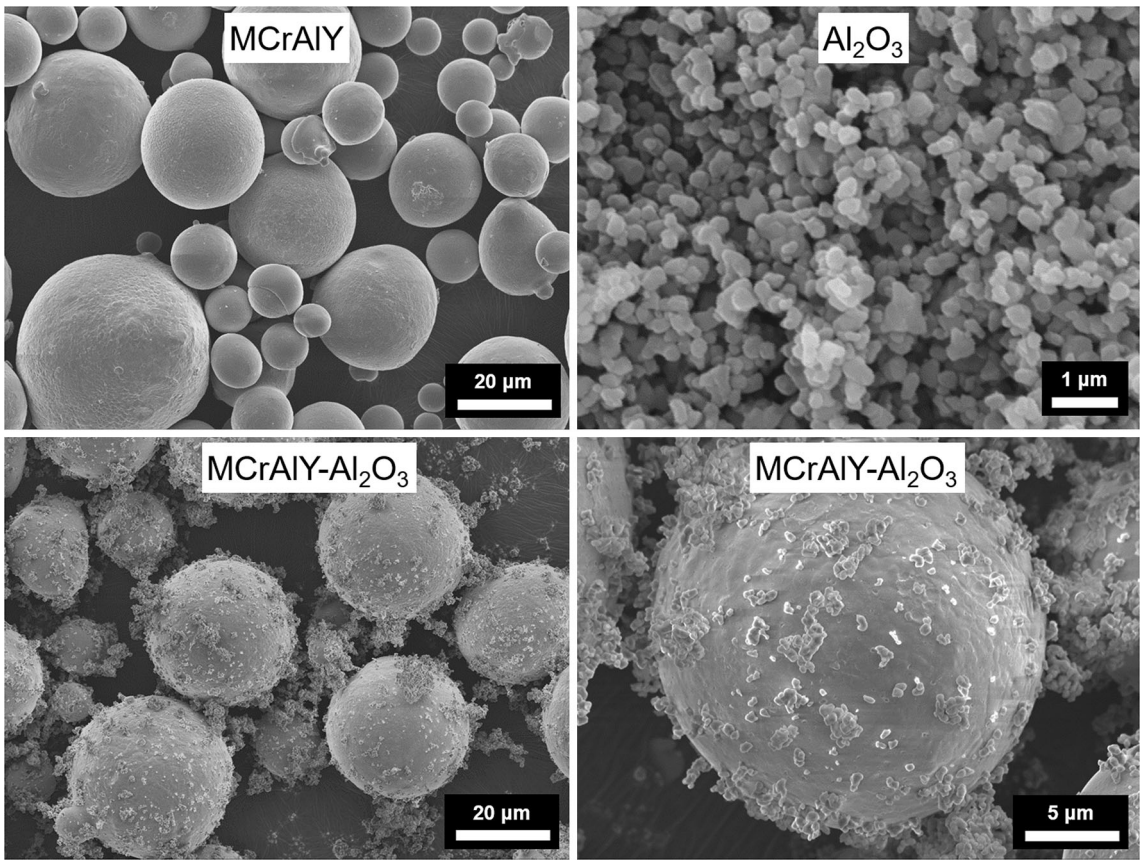

Fig. 1 SEM images of the feedstock powders: MCrAlY, Al_2O_3 and MCrAlY–Al_2O_3 composite under low and high magnification showing a good dispersion of Al_2O_3 with MCrAlY powder

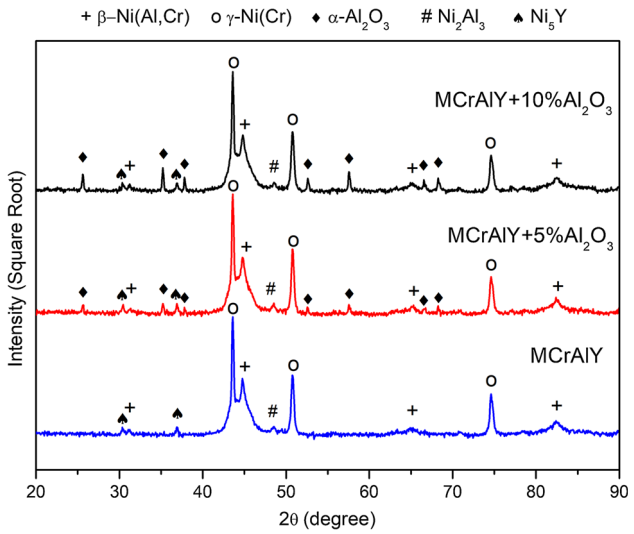

Fig. 2 XRD patterns of MCrAlY, MCrAlY + 5 wt.% Al_2O_3 and MCrAlY + 10 wt.% Al_2O_3 feedstock

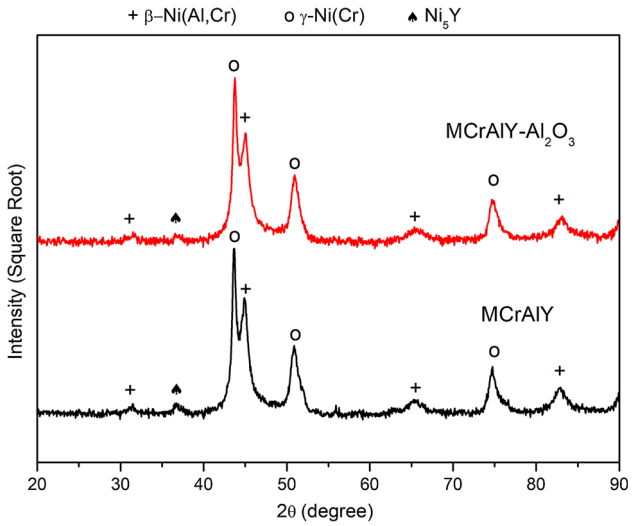

Fig. 3 XRD patterns of the as-sprayed MCrAlY and MCrAlY–Al_2O_3 composite coatings

with a minor amount of Ni_5Y phase. The presence of alumina is, however, not identified on the coatings surface, possibly because the content of alumina near the surface is less than 5 wt. % within the x-ray penetration depth range, which is approximately 3-5 μm for MCrAlY. The as-sprayed coatings were further examined by SEM and EDX for microstructure and composition.

Figure 4 shows the surface morphology and EDX elemental maps of the as-sprayed coatings. The surface features of both coatings are nearly identical consisting of molten splats and partially molten/unmolten MCrAlY particles. The compositions of the coatings surfaces are also very similar as indicated by the EDX semiquantitative analysis showing a majority of Ni, Cr and Al with a minor amount of O (6-7 wt.%) and Y (1-2 wt.%). An Y-rich area is also found on the composite coatings surface (marked by white arrow). The formation of these oxides is believed to be mainly caused by the inevitable oxidation during thermal spraying due to the interaction with atmospheric oxygen (Ref 18). This indeed makes the detection of the presence of original alumina particles even more difficult in contrast to the newly formed alumina.

Figure 5 shows the SEM images and EDX mappings with representative inter-lamella oxides on the cross sections of the two coatings. Both coatings are observed to be dense and uniform with the presence of a certain amount of inter-lamella oxides (dark phase), which are identified as alumina-rich oxide. The thickness, however, differed with $\sim$ 50% reduction in the composite coatings although both coatings were prepared under the same conditions. An enrichment of Cr is observed in the alumina-rich oxides in the MCrAlY coating, i.e., $(Al,Cr)_2O_3$, while the alumina-rich oxides in the composite coatings contain nearly no Cr but a higher level of Y. The formation mechanism for the different oxide compositions will be discussed later.

Oxidation analysis

Figure 6 shows the XRD analysis on the coatings surface after oxidation at 900 °C for 10 h. The peaks of both β and $\gamma(\gamma')$ phase are observed to be narrower compared to these of the as-sprayed coatings (Fig. 3), possibly due to the strain relaxation during oxidation. The presence of alumina is again difficult to identify as the composite coatings was unnoticeably oxidized with only a minor amount of spinel; while on the MCrAlY coatings surfaces, the peaks of NiO are more prominent together with the peaks of spinel oxide $(Ni(Al,Cr)_2O_4)$.

Figure 7 shows the surface morphology and EDX spectra of the oxidation products on the coatings top surface in BSE mode, together with the EDX elemental maps in Fig. 8. On the MCrAlY coatings surface, the area that appears to be brighter in contrast is identified as Ni-rich oxide (NiO), while dark area corresponds to the Al-rich oxide with the enrichment of Cr and Y. The bright oxides on the MCrAlY coatings (inset image) exhibited typical angular shape of NiO (Ref 39). On the other hand, the surface of the composite coatings appears to be uniformly dark contrast with wrinkled morphology. The EDX maps (Fig. 8) show that the oxides on the composite coatings are composed of mainly Al-rich oxide with nearly no Ni-rich oxide. This agrees with the XRD analysis as less NiO was identified on the composite coatings. The Al-rich oxide is believed to be alumina although the XRD failed to detect the presence of alumina probably because the oxide scale is too thin and falls under the detection limit of the XRD.

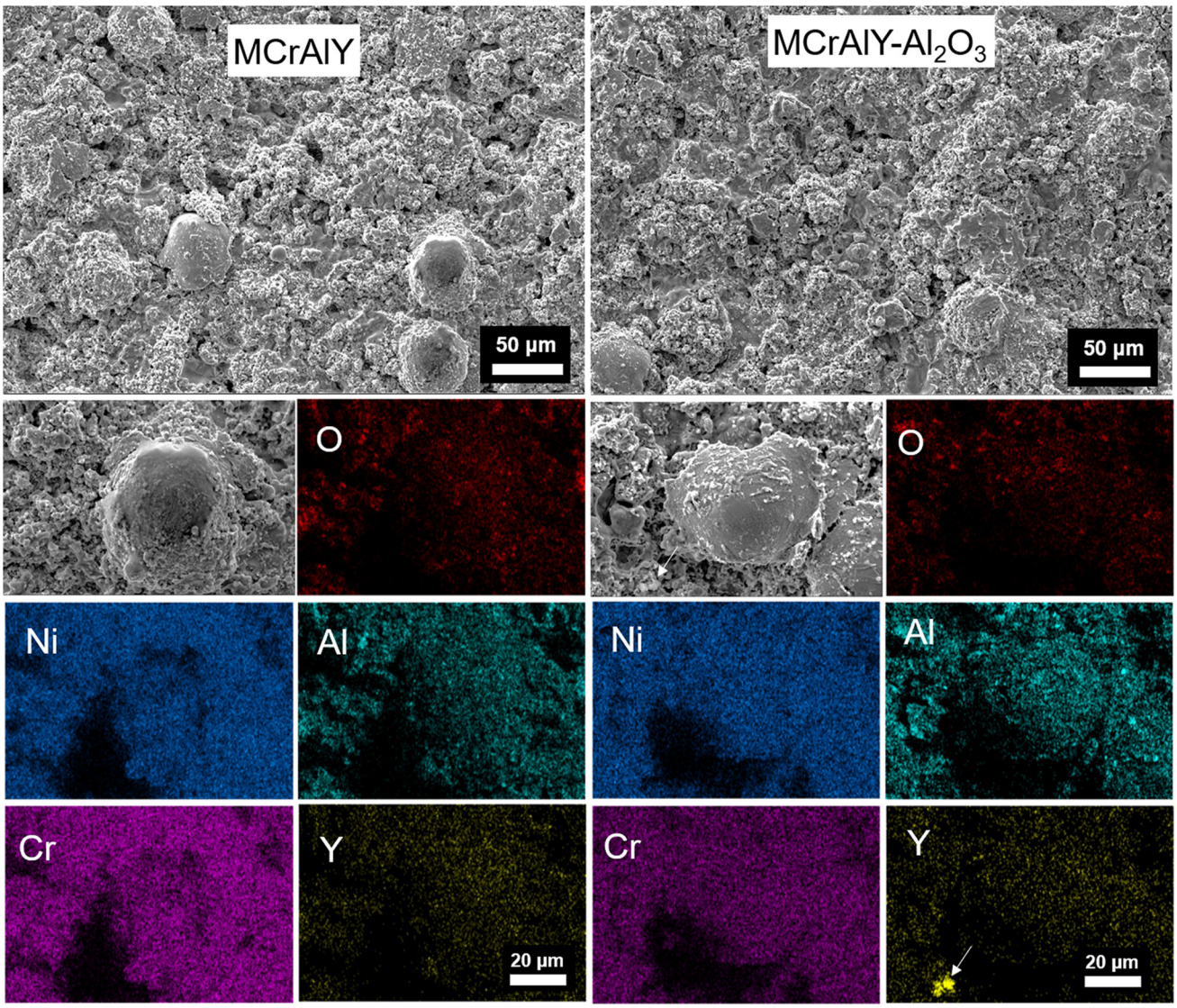

Fig. 4 SEM images and EDX mappings of as-sprayed MCrAlY and MCrAlY–Al_2O_3 composite coatings showing the surface morphology and compositions

Figure 9 shows the cross-sectional microstructure and compositions of the oxide scale on the two coatings. A coherent Al-rich oxide layer is observed on the composite coatings surface (right) with the thickness of less than 1 μm, while the oxides on the MCrAlY coatings (left) are composed of mixed compositions with Ni-rich, Cr-rich and Al-rich oxide throughout the coating. It is also worth noting that the oxidation analysis presented here was only based on short-term oxidation tests to evaluate the oxidation behavior of the newly developed composite coatings. However, for longer-term heat treatment, the oxidation resistance may differ as the Al element is depleted earlier in the thin coatings than the thick ones due to the continuous growth of Al_2O_3 and interdiffusion with the substrates. In addition, previous researches have suggested that the thickness of bond coat has an effect on the residual stress in the coatings and may lead to a different failure behavior (Ref 40). Thus, more complicated performance tests (e.g., thermal cycling) are still needed to fully examine the oxidation resistance of these composite coatings.

Discussions

The MCrAlY-based composite coatings reinforced by alumina or other refractory oxides (e.g., Y_2O_3, ZrO_2) have already been developed previously via different routes (Ref 41-45), and most of these studies were only focused on the wear performance of the composite coatings. This is

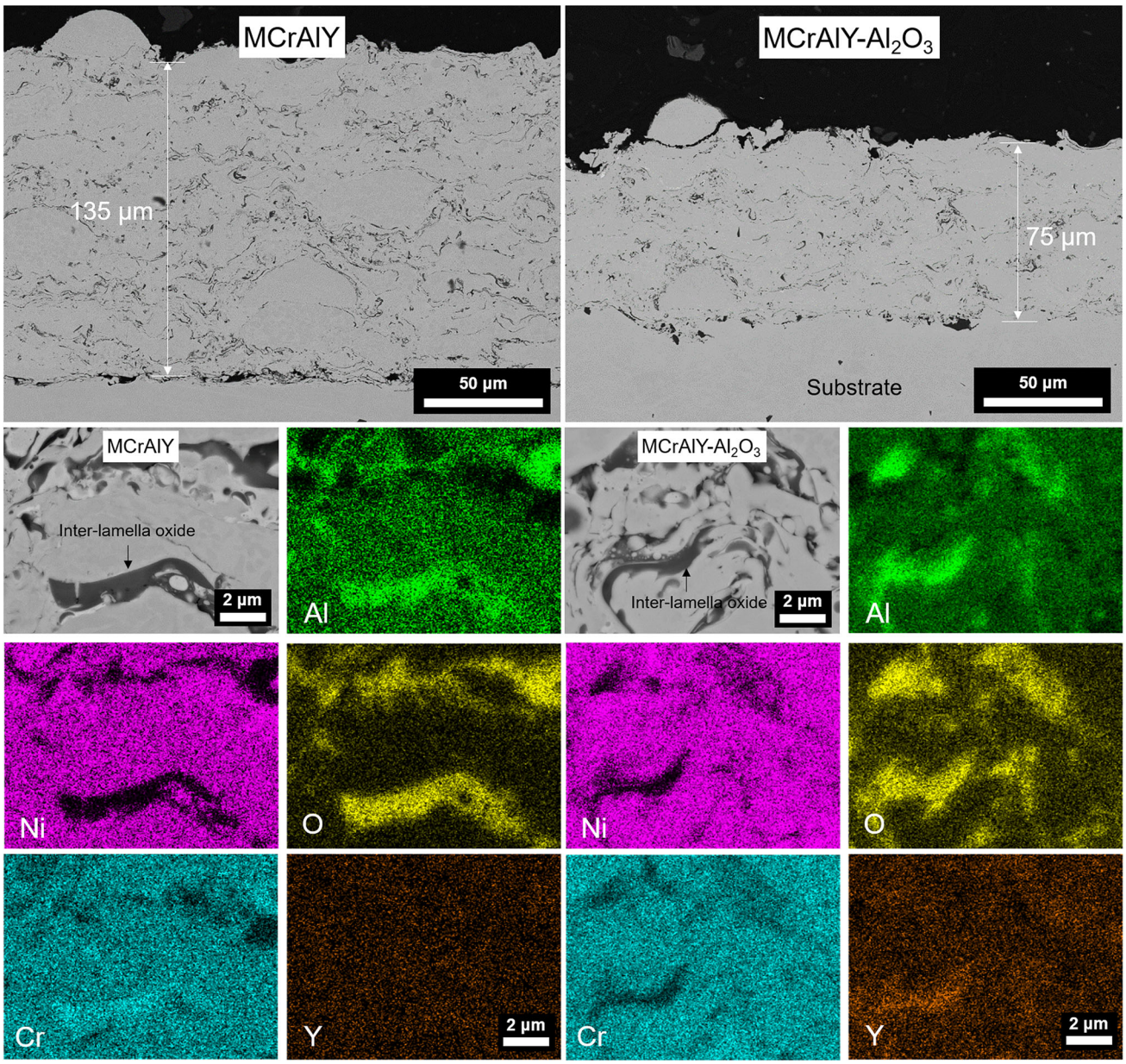

Fig. 5 SEM images and EDX mappings of representative inter-lamella oxides on the cross sections of as-sprayed MCrAlY and MCrAlY–Al_2O_3 composite coatings

because the addition of ceramic reinforcement hard phase into metallic coatings was primarily aimed at improving its mechanical strength against abrasion from room temperatures up to 800 °C, while the high-temperature oxidation behavior was only investigated by a few studies (Ref 46, 47). As a result, the beneficial effect of the alumina addition on the oxidation behavior of MCrAlY composite coatings has not been extensively investigated, especially at the early stages of oxidation. The experimental results in this study have demonstrated the improvement in the oxidation resistance with the formation of exclusive α-Al_2O_3 scale on the MCrAlY–Al_2O_3 composite coatings produced from the composite powder feedstock containing 5 wt.% of α-Al_2O_3 submicron particles. Although new Al_2O_3 also formed in between lamella and on the top surface during spraying due to the oxidation of MCrAlY powder, the original α-Al_2O_3 particles addition was still detectable by the EDX elemental analysis (Fig. 4 and 5) based on the different segregations of Y on the top surface and cross section of these two coatings. The EDX semiquantitative analysis gave the concentration of Y in the composite coatings (cross section: 1.6 wt.% and top surface: 1.2 wt.% based on three measurements) relatively higher than that of the MCrAlY coatings (cross section: 1.2 wt.% and top

surface: 1.0 wt.%). Since the starting concentration of Y in the MCrAlY powder was only 0.8-1.2 wt.%, it means that the relative concentration of Y in the selected area for EDX analysis of the composite coatings was increased 1/3 to 1/2. This is possible because the high specific surface area of the submicron alumina particles would significantly increase the probability of reaction with Y and O during spraying, forming stable YAG compounds ($Y_xAl_yO_z$) as a mixture of Y_2O_3 and Al_2O_3 leading to a locally higher Y content near the alumina particles. The presence of YAG was also observed by Toma et al. (Ref 48) in the HVOF thermally sprayed MCrAlY coatings doped with Al and Y metallic powders in the feedstock. Furthermore, Cr is another important indicator that could reveal the presence of the original α-alumina. The coexistence of Al and Cr is commonly seen in oxides (e.g., corundum) after oxidation of MCrAlY powders (Ref 18). The absence of Cr in the Al_2O_3-rich oxides in the composite coatings (Fig. 5) indicates that these lamella oxides in the composite coatings were retained from the original alumina particles that contain no Cr at all.

The selective oxidation of MCrAlY alloys mainly involves with the thermodynamic that can be explained in Fig. 10. It shows the calculation results of the oxide formation (mole fraction) on the MCrAlY coatings with the composition of Ni-23Cr-11Al-1.2Y as a dependency of O_2 partial pressures (atm) at 900 °C at equilibrium. Under low

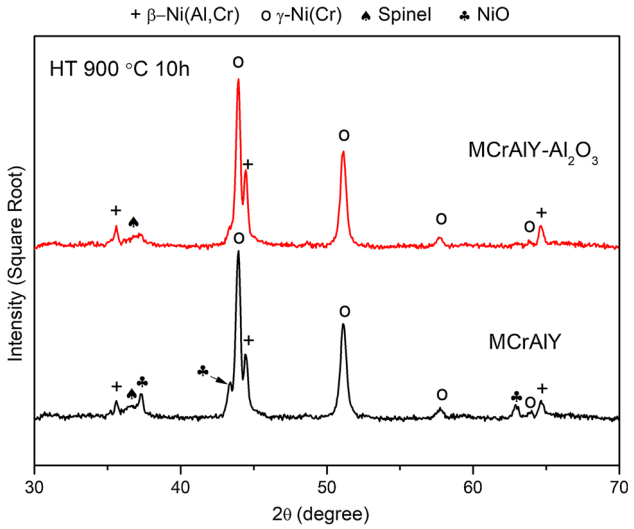

Fig. 6 XRD patterns of the oxidized MCrAlY and MCrAlY–Al_2O_3 composite coatings after short-term exposure to high-temperature treatment at 900 °C for 10 h

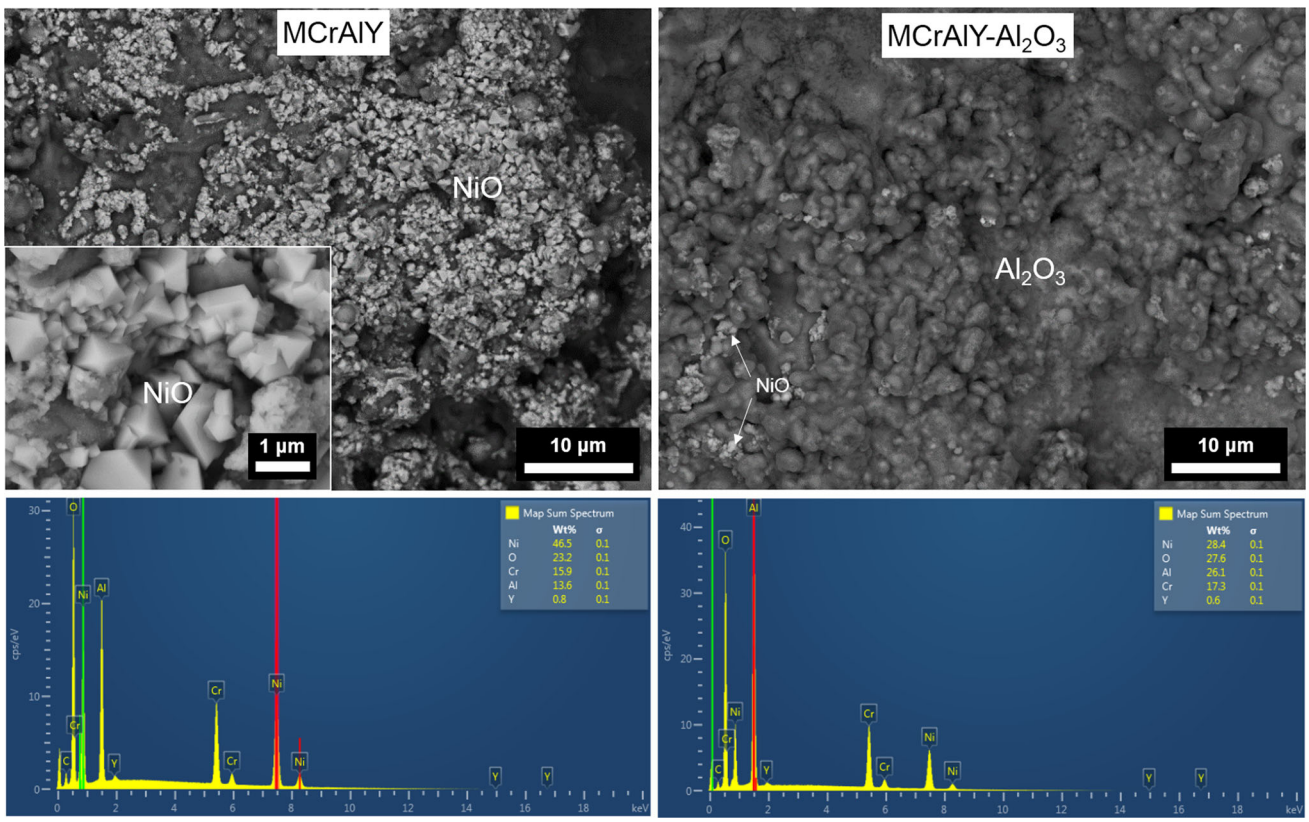

Fig. 7 SEM images (BSE) and EDX map spectra of the oxidation products on the surface of the oxidized MCrAlY and MCrAlY–Al_2O_3 composite coatings

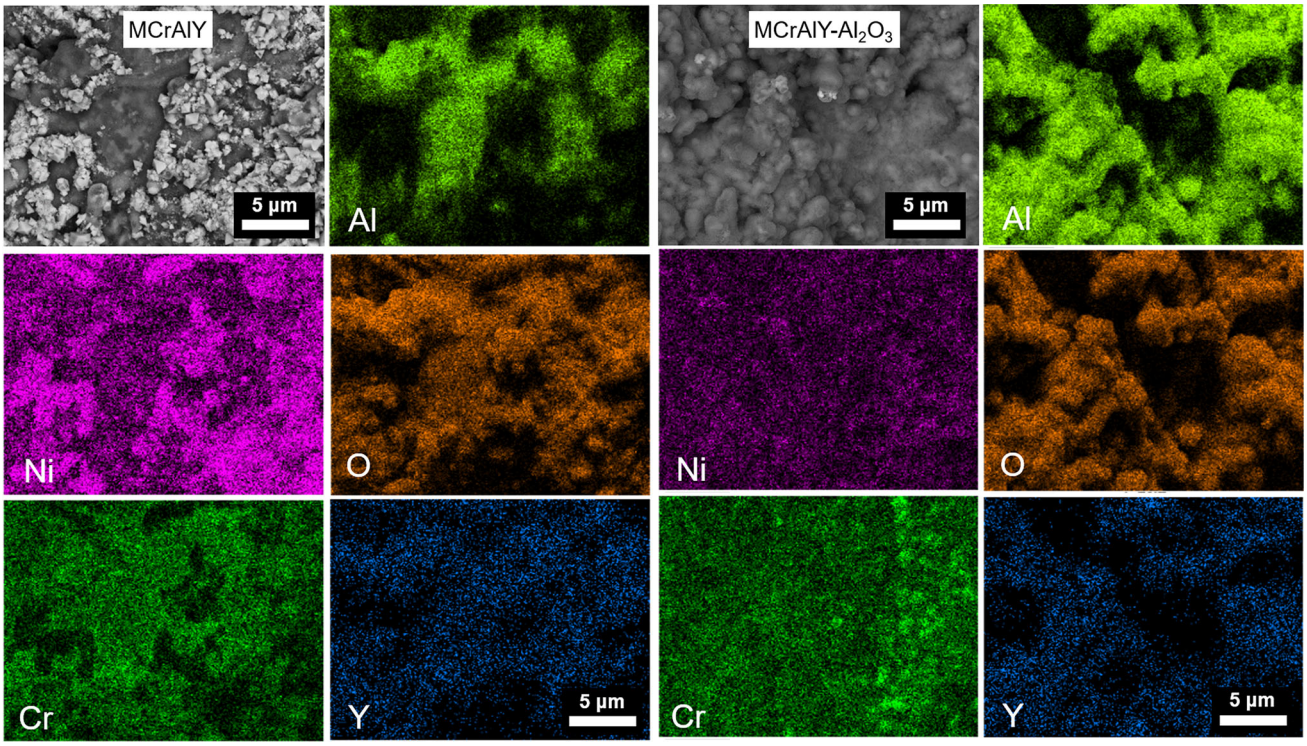

Fig. 8 SEM images (BSE) and EDX mappings showing the oxide composition on the surface of the oxidized MCrAlY and MCrAlY–Al_2O_3 composite coatings

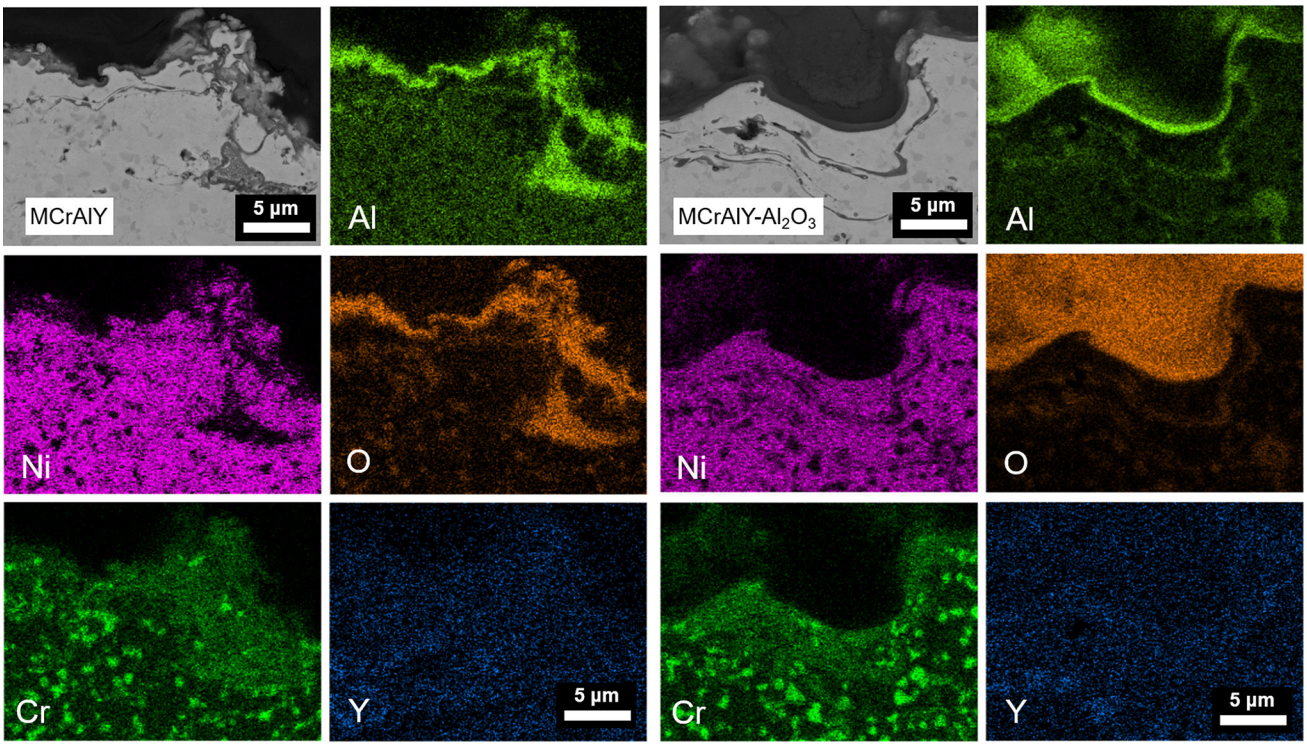

Fig. 9 SEM images (BSE) and EDX mappings of the oxide layer on the cross sections of the oxidized MCrAlY and MCrAlY-Al_2O_3 composite coatings

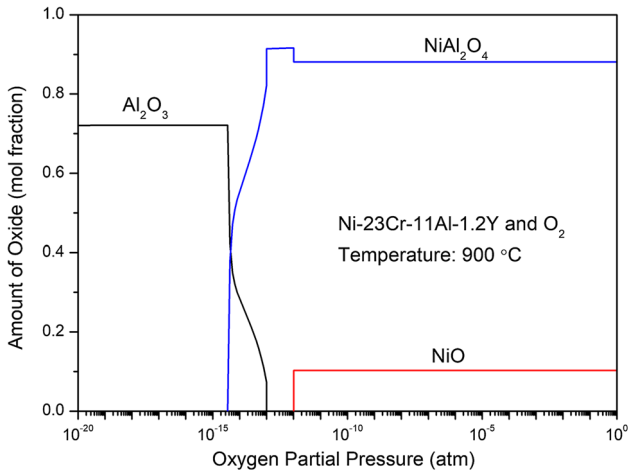

Fig. 10 Thermo-Calc® calculation of oxide formation (mole fraction) on MCrAlY coatings with the composition of Ni–23Cr–11Al–1.2Y as a dependency of O_2 partial pressures (atm) at 900 °C upon equilibrium. Thermo-Calc® (2017b) was used with TCNi8.1 database

pressure ($< 10^{-15}$ atm), both NiO and $NiAl_2O_4$ (spinel) are excluded due to the insufficient supply of O_2 but it promotes the formation of exclusive Al_2O_3. Once this Al_2O_3 forms first, it would further decrease the O_2 partial pressure and therefore avoid the formation of NiO and spinel. On the other hand, the formation of Al_2O_3 scale also slows down the diffusion of oxygen and metal ions through the dense oxide layer, which also kinetically inhibit the growth of other oxides and improve the oxidation resistance. Therefore, it is essential to obtain a coherent Al_2O_3 scale at the early oxidation scale.

The dispersion of α-Al_2O_3 particles, as a second phase, as well as other reactive element (RE) oxides, on the oxidation resistance of ODS (oxide dispersion strengthening) alloys have been discussed at length (Ref 49, 50). The mechanism involves with the dynamic-segregation theory (DST), in which these oxide dispersions mainly segregate at the oxide grain boundaries and oxide–metal interface (Ref 51). The segregations of α-Al_2O_3 and YAG oxide would hinder the outwards diffusion of undesirable outward cation transport (Ref 52). In particular, the diffusion coefficient of Al along the grain boundary of Al_2O_3 is several orders of magnitude higher than that of Ni and Cr [Al: 2.8×10^{-4} m^2/s; Cr: 6.9×10^{-11} m^2/s; Ni: 2.53×10^{-10} m^2/s (Ref 53)]. As a result, the growth of these non-protective spinel and NiO oxides would be greatly inhibited by the dispersed Al_2O_3 particles. The EDX semiquantitative results in Fig. 7 already showed that the Al content on the composite coatings top surface after oxidation (26.1 wt.%) is nearly twice that on the MCrAlY coatings (13.6 wt.%), while the initial compositions of both coatings prior to oxidation are nearly the same with the Al content being 10-11 wt.% and the Ni content being 62-63 wt.%. The increase in the Al content after oxidation indicates that the outwards diffusion of Al in the composite coatings during oxidation outperformed the competitive outwards diffusion of Ni. The element of Cr, on the other hand, remains a similar level (16-17 wt.%) in both coatings after oxidation (Fig. 7), and also, appears to be granular precipitates with an isolated and dispersed distribution, and a size of 1-2 μm inside the two coatings as shown earlier in Fig. 9. It implies that the Cr was less involved in the competitive outwards diffusion with Ni and Al during oxidation. In addition, the dispersion of the α-Al_2O_3 and YAG would act as the nucleation sites for the newly formed α-Al_2O_3 phase (Ref 15) and also suppress the formation of other transient metastable Al_2O_3 (e.g., θ, γ-Al_2O_3) or shorten its phase transformation to stable α-Al_2O_3 (Ref 54, 55). It would also inhibit interfacial void growth, thus improving scale adhesion. To summarize, the improved oxidation resistance of the composite coatings with accelerated outwards diffusion of Al is believed to be caused by the dispersion of the α-alumina particles, in combination with the YAG formation during spraying of the composite powder.

Conclusions

A detailed process has been introduced in this study for the preparation of MCrAlY–Al_2O_3 composite coatings via a suspension route followed by HVOF thermal spraying. A good distribution of alumina submicron particles was observed with the MCrAlY powders, and this, however, led to poor flowability for thermal spraying. Moreover, the presence of α-Al_2O_3 particles promoted the oxidation of Y during spraying forming YAG inter-lamella oxide. The composite coatings exhibited also superior oxidation resistance with the formation of nearly exclusively Al_2O_3 scale after short-term oxidation tests at 900 °C for 10 h in comparison with the MCrAlY coatings. The presence of α-Al_2O_3 particles in the composite coatings is believed to have accelerated the outwards diffusion of Al cations and inhibited Ni and Cr along the grain boundaries during oxidation, which therefore promoted the formation of Al_2O_3 scale.

Acknowledgment This work was supported by the Engineering and Physical Sciences Research Council (Grant Number EP/M01536X/1). The authors would like to acknowledge Mr. Rory Screaton for the experimental assistance in thermal spray. Dr. Mingwen Bai would also like to acknowledge many helpful discussions on power plant materials with Prof. Hao Liu and Prof. Wei Sun at the University of Nottingham during the USC-CFB-CMM project meetings.

References

1. H. Asteman and M. Spiegel, A Comparison of the Oxidation Behaviours of Al_2O_3 formers and Cr_2O_3 formers at 700 C–Oxide Solid Solutions Acting as a Template for Nucleation, *Corros. Sci.*, 2008, **50**(6), p 1734-1743
2. H. Josefsson, F. Liu, J.E. Svensson, M. Halvarsson, and L.G. Johansson, Oxidation of FeCrAl Alloys at 500-900 °C in Dry O_2, *Mater. Corros.*, 2005, **56**(11), p 801-805
3. J. Nicholls, Advances in Coating Design for High-Performance Gas Turbines, *MRS Bull.*, 2003, **28**(9), p 659-670
4. D. Naumenko, R. Pillai, A. Chyrkin, and W. Quadakkers, Overview on Recent Developments of Bondcoats for Plasma-Sprayed Thermal Barrier Coatings, *J. Therm. Spray Technol.*, 2017, **26**(8), p 1743-1757
5. R. Lima, D. Nagy, and B. Marple, Bond Coat Engineering Influence on the Evolution of the Microstructure, Bond Strength, and Failure of TBCs Subjected to Thermal Cycling, *J. Therm. Spray Technol.*, 2015, **24**(1-2), p 152-159
6. J. Bergholz, B.A. Pint, K.A. Unocic, and R. Vaßen, Fabrication of Oxide Dispersion Strengthened Bond Coats with Low Al_2O_3 Content, *J. Therm. Spray Technol.*, 2017, **26**(5), p 868-879
7. G. Mauer, D. Sebold, and R. Vaßen, MCrAlY Bondcoats by High-Velocity Atmospheric Plasma Spraying, *J. Therm. Spray Technol.*, 2014, **23**(1), p 140-146
8. T. Zhang, C. Huang, H. Lan, L. Du, and W. Zhang, Oxidation and Hot Corrosion Behavior of Plasma-Sprayed MCrAlY–Cr2O3 Coatings, *J. Therm. Spray Technol.*, 2016, **25**(6), p 1208-1216
9. N. Bala, H. Singh, S. Prakash, and J. Karthikeyan, Investigations on the Behavior of HVOF and Cold Sprayed Ni-20Cr Coating on T22 Boiler Steel in Actual Boiler Environment, *J. Therm. Spray Technol.*, 2012, **21**(1), p 144-158
10. S. Paul and M.D.F. Harvey, Corrosion Testing of Ni Alloy HVOF Coatings in High Temperature Environments for Biomass Applications, *J. Therm. Spray Technol.*, 2013, **22**(2), p 316-327
11. S. Hong, Y. Wu, G. Li, B. Wang, W. Gao, and G. Ying, Microstructural Characteristics of High-Velocity Oxygen-Fuel (HVOF) Sprayed Nickel-Based Alloy Coating, *J. Alloy. Compd.*, 2013, **581**, p 398-403
12. A.A. Khan, W. de Jong, P.J. Jansens, and H. Spliethoff, Biomass Combustion in Fluidized Bed Boilers: Potential Problems and Remedies, *Fuel Process. Technol.*, 2009, **90**(1), p 21-50
13. G.R. Holcomb, B.S. Covino Jr., S.J. Bullard, S.D. Cramer, M. Ziomek-Moroz, and D.E. Alman, *Ultra Supercritical Turbines–Steam Oxidation*, Albany Research Center (ARC), Albany, 2004
14. G.R. Holcomb, Steam Oxidation and Chromia Evaporation in Ultrasupercritical Steam Boilers and Turbines, *J. Electrochem. Soc.*, 2009, **156**(9), p C292-C297
15. H.J. Grabke, Oxidation of NiAl and FeAl, *Intermetallics*, 1999, **7**(10), p 1153-1158
16. D. Maghet, G. Marginean, I. Mitelea, A. Davidescu, and W. Brandl, *Comparison of oxidation behaviour of various thermally sprayed MCrAlY coatings*, The European corrosion congress, Breisgau, 2007
17. D. Utu, G. Marginean, V.-A. Serban, and C. Codrean, Corrosion Behavior of Laser Remelted CoNiCrAlY Based Composite Coatings, *Engineering*, 2010, **2**(05), p 322
18. W. Brandl, D. Toma, J. Krüger, H. Grabke, and G. Matthäus, The Oxidation Behaviour of HVOF Thermal-Sprayed MCrAlY Coatings, *Surf. Coat. Technol.*, 1997, **94**, p 21-26
19. Y.N. Wu, M. Qin, Z.C. Feng, Y. Liang, C. Sun, and F.H. Wang, Improved Oxidation Resistance of NiCrAlY Coatings, *Mater. Lett.*, 2003, **57**(16), p 2404-2408
20. Y.N. Wu, G. Zhang, Z.C. Feng, B.C. Zhang, Y. Liang, and F.J. Liu, Oxidation Behavior of Laser Remelted Plasma Sprayed NiCrAlY and NiCrAlY–Al_2O_3 Coatings, *Surf. Coat. Technol.*, 2001, **138**(1), p 56-60
21. G. Bolelli, A. Candeli, L. Lusvarghi, A. Ravaux, K. Cazes, A. Denoirjean, S. Valette, C. Chazelas, E. Meillot, and L. Bianchi, Tribology of NiCrAlY + Al_2O_3 Composite Coatings by Plasma Spraying with Hybrid Feeding of Dry Powder + Suspension, *Wear*, 2015, **344–345**, p 69-85
22. A. Clare and A. Kennedy, Additive Manufacturing. Google Patents, 2016.
23. H. Tan, D. Hao, K. Al-Hamdani, F. Zhang, Z. Xu, and A.T. Clare, Direct Metal Deposition of TiB 2/AlSi10 Mg Composites Using Satellited Powders, *Mater. Lett.*, 2018, **214**, p 123-126
24. F. Zhang, M. Mei, K. Al-Hamdani, H. Tan, and A.T. Clare, Novel Nucleation Mechanisms Through Satelliting in Direct Metal Deposition of Ti-15Mo, *Mater. Lett.*, 2018, **213**, p 197-200
25. K.S. Al-Hamdani, J.W. Murray, T. Hussain, A. Kennedy, and A.T. Clare, Cold Sprayed Metal-Ceramic Coatings using Satellited Powders, *Mater. Lett.*, 2017, **198**, p 184-187
26. M. Simonelli, N.T. Aboulkhair, P. Cohen, J.W. Murray, A.T. Clare, C. Tuck, and R.J.M. Hague, A Comparison of Ti-6Al-4 V In Situ Alloying in Selective Laser Melting Using Simply-Mixed and Satellited Powder Blend Feedstocks, *Mater. Charact.*, 2018, **143**, p 118-126
27. J. Bratberg, H. Mao, L. Kjellqvist, A. Engström, P. Mason, and Q. Chen, The Development and Validation of a New Thermodynamic Database for Ni-Based Alloys, *Superalloys*, 2012, **12**, p 803-812
28. J.O. Andersson, T. Helander, L. Höglund, P. Shi, and B. Sundman, Thermo-Calc & DICTRA, Computational Tools for Materials Science, *Calphad*, 2002, **26**(2), p 273-312
29. Z. Pala, M. Bai, F. Lukac, and T. Hussain, Laser Clad and HVOF-Sprayed Stellite 6 Coating in Chlorine-Rich Environment with KCl at 700 °C. Oxid. Met. 2017, p 1-23.
30. M. Bai, L. Reddy, and T. Hussain, Experimental and Thermodynamic Investigations on the Chlorine-Induced Corrosion of HVOF Thermal Sprayed NiAl Coatings and 304 Stainless Steels at 700 °C, *Corros. Sci.*, 2018, **135**, p 147-157
31. T.J. Nijdam and W.G. Sloof, Microstructural Evolution of a MCrAlY Coating Upon Isothermal Annealing, *Mater. Charact.*, 2008, **59**(12), p 1697-1704
32. K. Ma and J.M. Schoenung, Thermodynamic Investigation into the Equilibrium Phases in the NiCoCrAl System at Elevated Temperatures, *Surf. Coat. Technol.*, 2010, **205**(7), p 2273-2280
33. K. Ma, F. Tang, and J.M. Schoenung, Investigation into the Effects of Fe Additions on the Equilibrium Phase Compositions, Phase Fractions and Phase Stabilities in the Ni–Cr–Al System, *Acta Mater.*, 2010, **58**(5), p 1518-1529
34. J. Liang, H. Wei, Y. Zhu, T. Jin, X. Sun, and Z. Hu, Phase Stabilities in a NiCrAlYRe Coating Alloy, *Surf. Coat. Technol.*, 2012, **206**(11), p 2746-2750
35. J. Liang, H. Wei, Y. Zhu, X. Sun, Z. Hu, M. Dargusch, and X. Yao, Phase Constituents and Thermal Expansion Behavior of a NiCrAlYRe Coating Alloy, *J. Mater. Sci.*, 2011, **46**(2), p 500-508
36. B. Baufeld and M. Schmücker, Microstructural Evolution of a NiCoCrAlY Coating on an IN100 Substrate, *Surf. Coat. Technol.*, 2005, **199**(1), p 49-56

37. D.R.G. Achar, R. Munoz-Arroyo, L. Singheiser, and W.J. Quadakkers, Modelling of Phase Equilibria in MCrAlY Coating Systems, *Surf. Coat. Technol.*, 2004, **187**(2), p 272-283
38. L. Wu, R. Wu, P. Xiao, T. Osada, K. Lee, and M. Bai, A Prominent Driving Force for the Spallation of Thermal Barrier Coatings: Chemistry Dependent Phase Transformation of the Bond Coat, *Acta Mater.*, 2017, **137**, p 22-35
39. Y. Chen, X. Zhao, M. Bai, A. Chandio, R. Wu, and P. Xiao, Effect of Platinum Addition on Oxidation Behaviour of γ/γ' Nickel Aluminide, *Acta Mater.*, 2015, **86**, p 319-330
40. Y. Chen, X. Zhao, and P. Xiao, Effect of Microstructure on Early Oxidation of MCrAlY Coatings, *Acta Mater.*, 2018, **159**, p 150-162
41. B. Mann and B.J.W. Prakash, High Temperature friction and wear characteristics of various coating materials for steam valve spindle application, *Wear*, 2000, **240**(1-2), p 223-230
42. H.-Y. Wang, D.-W. Zuo, M.-D. Wang, G.-F. Sun, M. Hong, and Y.-L. Sun, High Temperature Frictional Wear Behaviors of Nano-Particle Reinforced NiCoCrAlY Cladded Coatings, *Trans. Nonferrous Met. Soc. China*, 2011, **21**(6), p 1322-1328
43. K. Bobzin, T. Schläfer, K. Richardt, and M. Brühl, Development of Oxide Dispersion Strengthened MCrAlY Coatings, *J. Therm. Spray Technol.*, 2008, **17**(5-6), p 853-857
44. L. Zhao, M. Parco, and E.J.S. Lugscheider, Technology, Wear Behaviour of Al_2O_3 Dispersion Strengthened MCrAlY Coating, *Surf. Coat. Technol.*, 2004, **184**(2-3), p 298-306
45. Y. Cao, C. Huang, W. Liu, W. Zhang, and L. Du, Effects of Boron Carbide Content on the Microstructure and Properties of Atmospheric Plasma-Sprayed NiCoCrAlY/Al_2O_3-B4C Composite Coatings, *J. Therm. Spray Technol.*, 2014, **23**(4), p 716-724
46. K. Ma, X. Tang, and J.M. Schoenung, Mechanistic Investigation into the Role of Aluminum Diffusion in the Oxidation Behavior of Cryomilled NiCrAlY Bond Coat, *J. Wuhan Univ. Technol. Mater. Sci. Edit.*, 2016, **31**(1), p 35-43
47. M. Okada, R. Vassen, M. Karger, D. Sebold, D. Mack, M.O. Jarligo, and F. Bozza, Deposition and Oxidation of Oxide-Dispersed CoNiCrAlY Bondcoats, *J. Therm. Spray Technol.*, 2014, **23**(1-2), p 147-153
48. D. Toma, W. Brandl, and U. Köster, The Characteristics of Alumina Scales Formed on HVOF-Sprayed MCrAlY Coatings, *Oxid. Met.*, 2000, **53**(1), p 125-137
49. D. Whittle and J. Stringer, Improvements in High Temperature Oxidation Resistance by Additions of Reactive Elements or Oxide Dispersions, *Philos. Trans. R. Soc. Lond. Ser. A Math. Phys. Sci.*, 1980, **295**(1413), p 309-329
50. B. Pint, Progress in Understanding the Reactive Element Effect Since the Whittle and Stringer Literature Review, in *Proceedings of John Stringer Symposium on High Temperature Corrosion*. ASM International Materials Park, Ohio, 2003, p. 9-19
51. B. Pint, Experimental Observations in Support of the Dynamic-Segregation Theory to Explain the Reactive-Element Effect, *Oxid. Met.*, 1996, **45**(1-2), p 1-37
52. J.G. Goedjen and D.A. Shores, The Effect of Alloy Grain Size on the Transient Oxidation Behavior of an Alumina-Forming Alloy, *Oxid. Met.*, 1992, **37**(3), p 125-142
53. L. Badrour, E.G. Moya, J. Bernardini, and F. Moya, Bulk Diffusion of 110Ag Tracer in Al_2O_3, *Scr. Metall.*, 1986, **20**(9), p 1217-1222
54. A. Vlad, A. Stierle, N. Kasper, H. Dosch, and M. Rühle, In Situ X-Ray Study of the γ- to α-Al_2O_3 Phase Transformation During Atmospheric Pressure Oxidation of NiAl(110), *J. Mater. Res.*, 2006, **21**(12), p 3047-3057
55. R. Cueff, H. Buscail, E. Caudron, C. Issartel, and F. Riffard, Oxidation Behaviour of Kanthal A1 and Kanthal AF at 1173 K: Effect of Yttrium Alloying Addition, *Appl. Surf. Sci.*, 2003, **207**(1), p 246-254